

Versatile and high temperature spectroscopic cell for *operando* fluorescence and transmission x-ray absorption spectroscopic studies of heterogeneous catalysts

Cite as: Rev. Sci. Instrum. **92**, 023106 (2021); <https://doi.org/10.1063/5.0038428>

Submitted: 22 November 2020 . Accepted: 15 January 2021 . Published Online: 19 February 2021

 Daniel Eggart,  Anna Zimina, Gülperi Cavusoglu,  Maria Casapu,  Dmitry E. Doronkin,  Kirill A. Lomachenko, and  Jan-Dierk Grunwaldt



View Online



Export Citation



CrossMark

ARTICLES YOU MAY BE INTERESTED IN

[Operando Fourier-transform infrared-mass spectrometry reactor cell setup for heterogeneous catalysis with glovebox transfer process to surface-chemical characterization](#)



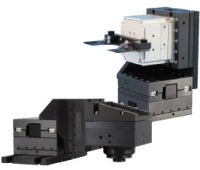
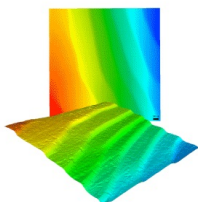
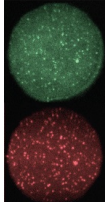
Review of Scientific Instruments **92**, 024105 (2021); <https://doi.org/10.1063/5.0041437>

[Optimal choice of multiple line-of-sight measurements determining plasma hotspot velocity at the National Ignition Facility](#)

Review of Scientific Instruments **92**, 023513 (2021); <https://doi.org/10.1063/5.0040319>

[Outline viewpoint feature histogram: An improved point cloud descriptor for recognition and grasping of workpieces](#)

Review of Scientific Instruments **92**, 025010 (2021); <https://doi.org/10.1063/5.0023164>

 MCL MAD CITY LABS INC. www.madcitylabs.com	<p>Nanopositioning Systems</p> 	<p>Modular Motion Control</p> 	<p>AFM and NSOM Instruments</p> 	<p>Single Molecule Microscopes</p> 
---	--	--	---	--

Versatile and high temperature spectroscopic cell for *operando* fluorescence and transmission x-ray absorption spectroscopic studies of heterogeneous catalysts

Cite as: Rev. Sci. Instrum. 92, 023106 (2021); doi: 10.1063/5.0038428

Submitted: 22 November 2020 • Accepted: 15 January 2021 •

Published Online: 19 February 2021



View Online



Export Citation



CrossMark

Daniel Eggart,¹  Anna Zimina,²  Gülperi Cavusoglu,¹ Maria Casapu,¹  Dmitry E. Doronkin,^{1,2} 
Kirill A. Lomachenko,³  and Jan-Dierk Grunwaldt^{1,2,a)} 

AFFILIATIONS

¹Institute for Chemical Technology and Polymer Chemistry (ITCP), Karlsruhe Institute of Technology (KIT), Engesserstraße 20, 76131 Karlsruhe, Germany

²Institute of Catalysis Research and Technology (IKFT), Karlsruhe Institute of Technology (KIT), Hermann-von-Helmholtz-Platz 1, 76344 Eggenstein-Leopoldshafen, Germany

³European Synchrotron Radiation Facility, 71 Avenue des Martyrs, CS 40220, 38043 Grenoble Cedex 9, France

^{a)} Author to whom correspondence should be addressed: grunwaldt@kit.edu

ABSTRACT

A modular high-temperature cell consisting of a plug-flow microreactor with a fixed catalyst bed and long heating zone has been established for *operando* x-ray absorption/fluorescence spectroscopic and diffraction studies. The functionality of the cell is demonstrated for two important areas: emission control using 2 wt. % Pd/Al₂O₃ acting as a three-way catalyst and direct conversion of methane to olefins and aromatics on a 0.5% Fe/SiO₂ catalyst. The performance has been determined by online infrared spectroscopy and mass spectrometry, respectively. In addition, the cell can be combined with optical spectroscopy, such as Raman spectroscopy. The catalyst, present as powdered/sieved samples, can be measured under reaction conditions at temperatures of up to 1050 °C. Another key aspect is a long isothermal heating zone with a small temperature gradient (<3 °C/mm at 1000 °C without reaction) including an inert zone for pre-heating of the reactant gas. Due to the small size of the microreactor and the heating system including a water cooling system, heating/cooling rates of up to 100 °C/min can be achieved. Moreover, due to the compact design and the autonomous control system, the high temperature *operando* setup fits to the space at the majority of synchrotron beamlines. In many cases, the concentration of the element of interest in the catalysts is low requiring x-ray absorption spectroscopy measurements in the fluorescence measurement mode. Hence, the microreactor was designed to fit such needs as well. More specifically, the case of Fe-containing catalysts was particularly considered by using iron-free materials for the reactor housing.

© 2021 Author(s). All article content, except where otherwise noted, is licensed under a Creative Commons Attribution (CC BY) license (<http://creativecommons.org/licenses/by/4.0/>). <https://doi.org/10.1063/5.0038428>

I. INTRODUCTION

Understanding heterogeneous catalysts in terms of interactions between the active sites and the support, activation, and deactivation pathways as well as regeneration conditions is key for improved design and development of highly active and stable catalysts.^{1–5} These questions are best answered with characterization methods that allow measurement of catalysts under reaction conditions.^{6,7} In this regard, x-ray absorption spectroscopy (XAS) is a highly suitable method for *operando* investigation of heterogeneous catalysts under

realistic conditions due to the high penetration depth of the high-energy x rays.^{8–12} Variations in oxidation states and local geometry of active sites can be derived from the x-ray absorption near edge structure (XANES) data, whereas detailed information on the coordination environment, such as the type of neighbors, interatomic distances, and coordination numbers, can be obtained by analysis of the extended x-ray absorption fine structure (EXAFS) data.^{11,12} For example, a reduction protocol to vary the size and dispersion of Pt nanoparticles on CeO₂ in order to tune the catalytic activity

for total oxidation reactions was proposed with the help of *operando* XAS.¹³ Moreover, XAS can be easily combined with other *operando* methods in order to acquire complementary information about the crystalline structure of the support or nature of the adsorbed species, for instance.^{9,14} This approach was, for example, applied to study the hydrocarbon activation step during selective oxidation of propene by bismuth molybdates with combining *operando* XAS and x-ray diffraction (XRD)/Raman spectroscopy and led to a holistic understanding of the multicomponent catalyst redox behavior influencing the catalytic performance.¹⁵

During the last few decades, a wide array of XAS cells has been developed to measure catalyst powders or pellets at elevated temperatures (of >750 °C) under a reaction gas atmosphere.^{12,16–22} In each of these designs, the best compromise between the optimal performance in spectroscopy and catalysis must be found.^{10,23} To overcome pore diffusion problems occurring while measuring pellets, a commonly used plug-flow setup features sieved catalysts placed between two quartz wool plugs in a quartz capillary heated by a gas blower.²³ This concept was first introduced by Clausen *et al.*²⁴ and Sankar *et al.*²⁵ It has been further developed by Grunwaldt *et al.*²³ and allows the combination of XAS with scattering techniques [XRD; small angle x-ray scattering (SAXS)] and optical spectroscopies, for instance, UV–Vis, Raman spectroscopy, and IR thermography.²⁶ In our experience, achieving temperatures above 800 °C and avoiding temperature gradients over the catalytic bed are challenging with a capillary microreactor heated by a gas stream blower. Gradients at temperatures below 700 °C have been circumvented using special housings. To overcome these difficulties, several alternatives have been more recently proposed by various research groups. Higher temperatures of up to 1000 °C can be reached with a cell developed by Aguilar-Tapia *et al.*²⁷ In this setup, the sample is placed within a glassy carbon tube heated by the surrounding molybdenum wires where the He atmosphere protects both from oxidation. In general, glassy carbon has a higher transmittance of x rays than quartz but is more easily corroded by oxidative gas atmospheres, limiting the feasible reaction gas atmospheres. An alternative plug-flow microreactor first introduced by Chupas *et al.*²⁸ and then improved by Figueroa *et al.*²⁹ focuses IR radiation of two Kanthal® A-1 heating wire coils with a circular aluminum shield around a quartz capillary. Thereby, a low axial temperature gradient along the catalyst bed at a maximum operating temperature of about 900 °C has been reported.²⁹ The relatively large front openings allow measurement of x-ray absorption, fluorescence, and XRD but have to be covered by Kapton tape to reduce temperature fluctuations by air circulation.²⁹ Andrieux *et al.*³⁰ introduced an advanced cell design for *operando* XRD measurements with the sample placed in a sapphire tube heated by Fe–Ni–Cr Kanthal wires up to 1000 °C. The sample can be rotated by a goniometer, and the unique gas dosing system allows pressure ranges of 10^{−3} mbar–200 bar.

In addition to providing the desired reaction conditions, i.e., high temperature, low temperature gradients along the catalyst bed, and plug-flow geometry, an advanced *operando* cell for XAS studies should also be applicable to study catalysts with a low content of the active species. Such metal-based catalysts are often applied for relevant industrial processes. For instance, Fe single-sites supported on silica (<1 wt. % Fe loading) gained increasing attention due to their high activity in the direct conversion of methane to

ethylene and aromatics at temperatures above 950 °C.^{31–35} However, their structure under operating conditions is strongly discussed and x-ray absorption spectroscopy (XAS) would be an ideal technique to investigate this. A similar situation is encountered in the case of emission control catalysts, which typically contain small amounts of Pt, Pd, and/or Rh supported on γ -Al₂O₃ and Ce_xZr_yO_z.³⁶ Despite the fact that they have been exploited for decades in real applications, detailed structure–activity relationships still need to be derived in order to improve their activity and comply with stricter emission regulations. However, measuring *operando* XAS on such catalysts is challenging because of the broad temperature window (up to 1000 °C) and highly absorbing carrier components, as, for example, demonstrated for Pt–CeO₂-based catalysts.^{13,37} Analogously, *operando* XAS investigation on samples with low loading of iron is even more difficult, as iron in stainless steel or aluminum from the sample surroundings tends to interfere with the fluorescence signal of the measured sample. None of the so far introduced setups allows XAS measurements in the fluorescence mode of samples with a low iron content of less than 1 wt. % at elevated reaction temperatures of up to 1000 °C. Hence, here we present an *operando* plug-flow microreactor specifically designed to sustain high temperatures of up to 1050 °C for several days, low heat capacity for rapid heating/cooling, and long isothermal zone and, finally, to reduce Fe x-ray fluorescence (XRF) noise by minimizing the Fe content in the reactor housing and shielding the x-ray beam from iron containing parts. The aim is to use modular components to allow the combination of different *operando* methods as well as a user-friendly assembly for switching between the measurement methods. The reactor design targeted not only a small size but also manufacturing at a rather low cost with a simple heating system compared to, e.g., rather cost-intensive and complex high temperature gas blower systems.

II. DESCRIPTION OF THE SPECTROSCOPIC OPERANDO CELL

A. Operando cell with fixed-bed microreactor

The 3D layout of a new plug-flow reactor, inspired by the earlier designs described in the Introduction and particularly by the setup in Ref. 29, is shown in Fig. 1. The basic principle is the use of heating wires for reactor heating, a quartz or similar capillary as a plug-flow reactor, and adjustment of the sample in the middle by a linear motion guide. During the design of the cell, special attention was paid to the modular components, which were optimized for an easy-to-handle configuration of the setup while allowing *operando* x-ray transmission and fluorescence as well as diffraction measurements. Several iron-free materials were evaluated for the oven housing with respect to their melting point, IR reflectivity, and ease of machining. Thereby, copper was chosen due to its high IR reflectivity of about 98%³⁸ and melting point of 1083 °C.³⁹ Interchangeable shielding windows allow not only user-friendly switching, but also combination of the characterization methods. For fluorescence measurements, the front window is closed and the side windows can vary in diameter depending on the detector size [Fig. 1(a)]. High-energy diffraction measurements are possible with the front window fully open giving a 2 θ range of 8.5° [Fig. 1(c)]. Furthermore, x-ray spectroscopy can be coupled with optical spectroscopy, such as Raman spectroscopy. Filling of the plug-flow microreactor, the heating/cooling system, and the linear motion guide are described in the

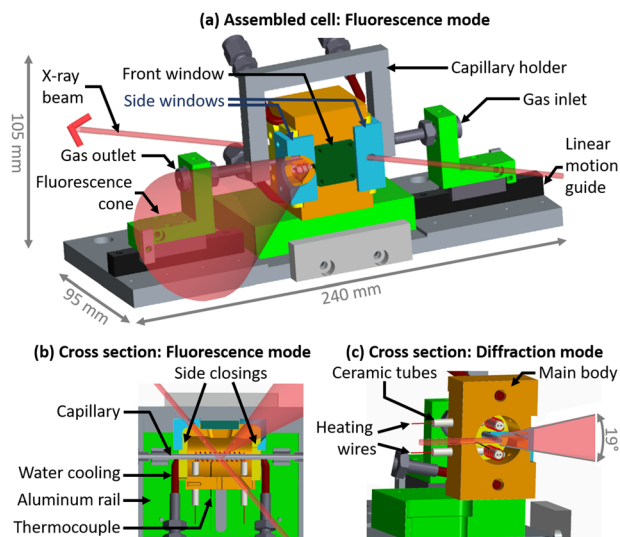


FIG. 1. 3D layout of the (a) fully assembled microreactor setup in the XAS fluorescence mode [side windows open (cyan), front shielding window (green), capillary as key for the fixed bed reactor and capillary holder, the oven body (orange) with heating wires, and water cooling system (red) mounted on a rail for alignment] and (b) cross section view thereof; (c) cross section view of the microreactor in the diffraction mode (side windows closed, front window open).

following. Note that the whole assembly is mounted on an xyz table or a hexapod system to adjust it in the synchrotron beam and has been tested at various beamlines (e.g., P65 at DESY⁴⁰ and CAT-ACT at KIT⁴¹).

For preparation of the microreactor, the sieved catalyst material (grain size typically 50 μm –250 μm) is placed between two quartz wool plugs in a quartz capillary [0.5 mm–3 mm outer diameter (OD) and 10 μm –40 μm wall thickness, WJM-Glas Müller GmbH]. The microreactor is then sealed airtight in an aluminum capillary holder [Fig. 1(a)] with high-temperature epoxy glue (LOCTITE[®] EA 3450, Henkel), similarly to the one described in Ref. 42. The setup can be used at pressures of at least 20 bars.⁴³ The capillary diameter is selected depending on the x-ray transmission through the sample and can also be used to adjust the gas hourly space velocity (GHSV). The wall thickness depends on the incident x-ray energy as well as the intended pressure range of the reaction gas. The capillary holder is mounted on a linear motion guide (THK GmbH, SRS-G) enabling precise positioning of the catalyst bed in the middle of the reactor [Fig. 1(a)]. Through Swagelok[®] fittings attached to the capillary holder, the connections to a gas dosing and to a gas analysis system are possible. Additionally, several capillary holders allow for pre-arrangement of the capillaries and thereby accelerated exchange of the samples during beamtime. Once the capillary holder is fixed, the main reactor body can be slid on an aluminum rail over the capillary [Fig. 1(b)]. The rail is fixed on an aluminum plate, which can be positioned on any movable stage available at the beamline for the alignment of the cell to the beam. The fully assembled cell is relatively small (240 \times 95 \times 105 mm³; length \times width \times height), weighs about 2 kg, and therefore fits to the space available for the sample environment at the majority of beamlines. An image of the working

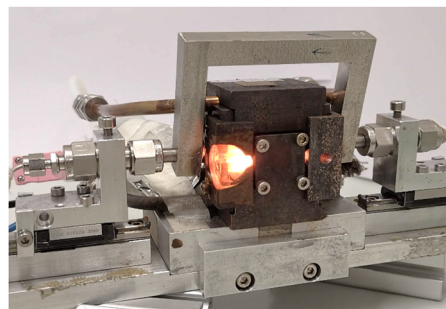


FIG. 2. Image of the microreactor at 975 °C reaction temperature with the windows arranged for XAS measurements in the fluorescence mode and the side window closed with Kapton tape.

reactor at 975 °C can be seen in Fig. 2. Additional images and drawings of the microreactor are given in Figs. S1–S4.

B. Heating system

The low-weight heating/cooling system is a key part of the *in situ* microreactor. For this purpose, heating wires (Kanthal A1, 1.0 mm diameter, EWWK GmbH, NT0019-H) are coiled around a ceramic tube (4 mm OD \times 28 mm long, Aliaxis Deutschland GmbH, F143-11040-00028) and isolated from the main oven body by ceramic tubes (Aliaxis Deutschland GmbH, F122-11004-00025) [Fig. 1(c)]. 16 windings equally distanced for each coil are connected in parallel and give an average resistance of 1.3 Ω at room temperature. Instead of using a 0.5 mm diameter resistive wire as reported by Chupas *et al.*,²⁸ a thicker wire of 1.0 mm diameter was used prolonging its lifetime at elevated operation temperatures. In order to circumvent gas conversion by thermocouples, the thermocouple (N-type, 0.5 mm diameter, TC Mess-und Regeltechnik GmbH, 406-601) is positioned outside the capillary inside the oven closely to the center of the catalyst bed [Fig. 1(b)]. The thermocouple is fixed to the reactor main body with a screw, and accidental removal is prevented by a clamp fixed to the slide rail. An additional thermocouple can be put inside the capillary in direct contact with the catalyst bed through a ferrule in a Swagelok Tee piece for the direct temperature calibration. The resistive wires of two heating coils (above and below the microreactor) are connected in series to a direct current supply (Delta Elektronika, SM 70-AR-24-P258, max. 0–35 V/0–24 A/800 W), and the temperature is regulated by a Eurotherm 2416 controller (heating output between 0 V and 5 V). The capillary is positioned in the center of the main body's cavity between the two coils and is therefore homogeneously heated by the focused IR radiation. Sudden temperature changes are avoided through minimization of air circulation by closing the window's apertures with Kapton tape. Thereby, a maximum temperature in the capillary of 1050 °C can be reached and maintained for several days. The temperature of the cell's outer body does not exceed 100 °C below 800 °C operating temperature due to passive air cooling (convection). Above 800 °C operating temperature, water cooling is necessary to prevent possible overheating of the beamline components (e.g., the piezo-motors of a hexapod positioning system installed at the CAT-ACT beamline at KIT's synchrotron radiation source) and of the Be window of

the fluorescence detector. With water cooling at 23 °C, heating and cooling rates of up to 100 °C/min can be realized.

C. Temperature profile in the heating zone

The reaction rates over catalysts are strongly dependent on the temperature. Hence, a stable and homogeneous temperature profile along the catalyst bed is required for *operando* spectroscopic experiments. In addition, the overall x-ray absorption and edge jump of the element of interest needs to be adjusted. Hence, depending on the penetration depth of the x rays and the concentration of the investigated element, capillaries of different diameters were used. Usually, diameters of 1 mm–2 mm have given the best results for *operando* transmission XAS measurements. Considering the use of a sieve fraction of 100 μm , adjustment of the gas flow vs catalyst bed volume/mass thereby results in a catalyst bed length of 5 mm–10 mm. For the *operando* XAS measurements reported in this study, the applied catalyst bed length was 6 mm for capillaries of 1.5 mm diameter. Temperature profiles were recorded by pulling a thermocouple (0.25 mm diameter) fixed on a movable stage out of a capillary (1.5 mm O.D.) with the catalyst bed fixed between two quartz wool plugs. Temperature distributions at a 400 °C and 1000 °C setpoint with the water cooling system in use along a 40 mm catalyst bed of 2.5% Pt/CeO₂ (100 μm –200 μm sieve fraction) at 5 ml/min and 50 ml/min He flow are shown in Fig. 3. The average axial temperature gradient varies within the area of interest (over 6 mm bed length centered in the microreactor, Fig. 3) depending on the gas flow with about 2.2 °C/mm (5 ml/min) and 2.7 °C/mm (50 ml/min) at 1000 °C. At 400 °C, the average axial temperature gradient for 6 mm bed length alters from 1.5 °C/mm (5 ml/min) to 1.8 °C/mm (50 ml/min). We conclude that the temperature homogeneity is very good in this microreactor; we expect that mostly the applied gas flow and reaction enthalpy (exothermic/endothermic reaction) have a more pronounced effect on the temperature gradient and should be, e.g., determined by an IR camera.^{44,45} Compared to the design by Figueroa *et al.*,²⁹ using aluminum instead of copper yields a lower axial temperature gradient of ≈ 0.13 °C/mm at

temperatures above 670 °C due to a lower heat loss on the basis of lower heat conductivity of Al (237 W/m K) than Cu (401 W/m K).⁴⁶ Some reduction of axial temperature gradient of the proposed cell could be achieved by heating of the gas inlet pipes. Furthermore, addition of insulating ceramic parts with apertures for the heating wires and x-ray windows would further reduce the heat loss. Nevertheless, in comparison to microreactor setups with commercial gas blowers, the temperature is more homogeneous over a larger section of the microreactor. In addition, in the present setup, the reactant gas can be sufficiently pre-heated in the zone before entering the fixed bed containing the catalyst. Challenges with this reactor remain with respect to the brittleness of the capillary, especially if only 10 μm thin quartz capillaries need to be used and that in the case of too long beds a plugging and thus a too high-pressure drop may occur. The aspect of brittleness is minimized by fixing the capillaries to the capillary holder with epoxy glue (similar to Ref. 42). However, after prolonged heating (>10 h) with temperatures exceeding 900 °C, the epoxy glue tends to get very rigid and the capillary can only be removed from the capillary holder by breaking it off (see the [supplementary material](#) for more detailed discussion). Since the temperature regulation is highly sensitive to the position of the thermocouple, the temperature should be recalibrated after every assembly of the setup.

D. Fluorescence XAS measurements of samples with iron loading below 1 wt. %

One of the further main objectives for this setup is to enable the XAS measurements in the fluorescence mode of samples with low iron loading at temperatures of up to 1000 °C without interference signals from the surrounding Fe-containing environment. For this purpose, the housing of the oven has been made of iron-free Cu-ETP [energy-dispersive x-ray spectroscopy (EDX) measurement cf. Fig. S5, XRF measurement cf. Fig. S6] instead of aluminum.²⁹ At the same time, the N-type thermocouple sheath is made of iron-free Nichrotherm DTM, and finally, the iron containing Kanthal A1 heating wire (iron–chromium–aluminum alloy⁴⁷) is protected from

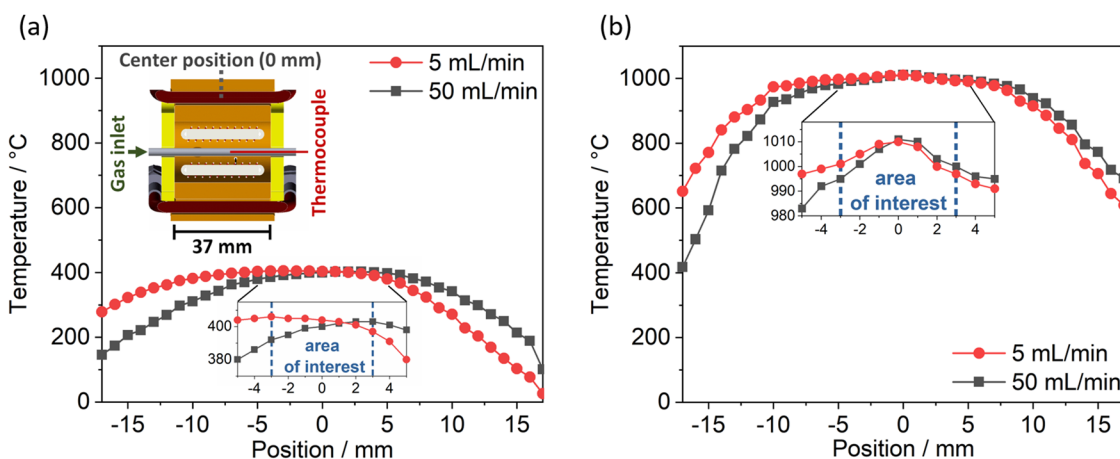


FIG. 3. Temperature profile at a setpoint of (a) 400 °C and (b) 1000 °C along a 40 mm catalyst bed filled with 2.5 wt. % Pt/CeO₂, 100 μm –200 μm sieve fraction, quartz capillary 1.5 mm OD, and 20 μm wall thickness at 5 ml/min and 50 ml/min He flow; center of the microreactor at 0 mm and gas inlet at about –25 mm position; area of interest for determination of the temperature gradient from –3 mm to +3 mm; inset of (a): cross section of the microreactor.

x rays through the arrangement of the windows. The entrance window of the x-ray fluorescence detector can be shielded with iron-free copper sheets instead of aluminum foil to reduce Fe fluorescence background signals from the surrounding equipment at the beamline. With the proposed cell design, it was possible to measure Fe K_{α} x-ray fluorescence of a 0.04% Fe/SiO₂ sample with 90% of the fluorescence signal originating from the sample (cf. Fig. S7). The residual x-ray fluorescence Fe background signals most likely originated from the surrounding beamline equipment and not from the microreactor setup (cf. Fig. S7). Therefore, the proposed arrangement gave the best compromise between the low Fe x-ray fluorescence noise and the optimal temperature profile along the catalyst bed.

III. APPLICATION: XANES/EXAFS INVESTIGATIONS

A. Experimental

XAS measurements were conducted at the P65 beamline of the PETRA III synchrotron radiation source (DESY,

Hamburg) in the transmission mode using ionization chambers for Pd K-edge (24.350 keV) and combining transmission/fluorescence mode using an additional 7 pixel HPGe detector (Canberra GmbH) for Fe K-edge (7.112 keV).⁴⁰ The source of x rays is an 11 period undulator, and higher harmonics were rejected by a pair of plane mirrors (Si for Fe K-edge and Pt-coated Si for Pd K-edge) installed in front of the monochromator. The energy of x-ray photons was further selected by Si(111) for Fe K-edge and Si(311) for Pd K-edge double-crystal monochromators, and the beam size was set with slits to $1.0 \times 0.2 \text{ mm}^2$. XANES spectra were recorded in the rapid continuously scanning mode, and EXAFS spectra were acquired in the step scanning mode. The spectra were processed using the ATHENA program from the Demeter software package.⁴⁸ The catalyst powder (sieved fraction size = $100 \mu\text{m}$ – $200 \mu\text{m}$) was loaded in a quartz capillary (100 mm length, outer diameter = 1.5 mm, and wall thickness = 0.02 mm) and fixed between two quartz wool plugs. Gases were dosed with the mass flow controllers (Bronkhorst) and analyzed with either the mass spectrometer (MS, Pfeiffer Vacuum, OmniStar GSD 320 T) or the online Fourier-transform infrared spectrometer (FTIR,

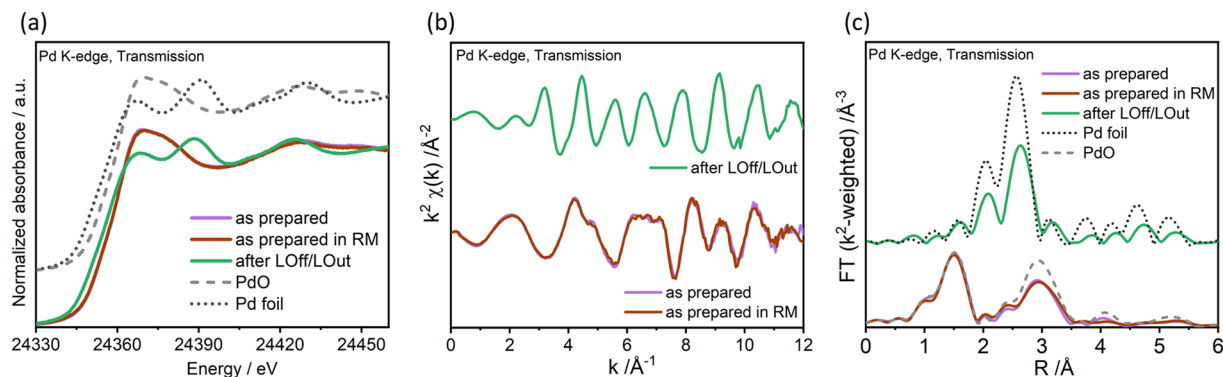


FIG. 4. (a) Pd K-edge XANES spectra and EXAFS refinement data in (b) k - and (c) R -space (not corrected for phase shift) before and after light-off/light-out cycle recorded at room temperature under state steady conditions after following *operando* treatment: as prepared, as prepared in the reaction gas mixture, and after light-off/light-out.

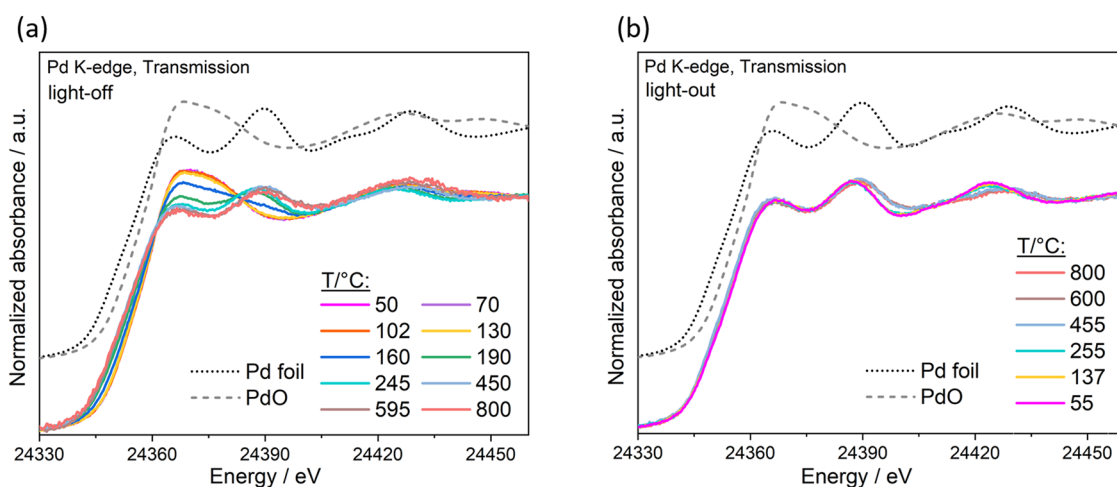


FIG. 5. Normalized Pd K-edge XANES spectra for the 2 wt. % Pd/Al₂O₃ catalyst and for PdO and Pd foil as references recorded during (a) light-off and (b) light-out under stoichiometric three-way reaction conditions, $\lambda \approx 1$ (3000 ppm CO, 1000 ppm NO, 1000 ppm C₃H₆, 5400 ppm O₂, 3% H₂O, and He in balance).

MKS, Multigas MG2030). The exhaust gas lines were heated to 150 °C.

The 2 wt. % Pd/Al₂O₃ three-way catalyst (TWC) was prepared by the incipient wetness impregnation method using palladium acetylacetonate (STREM Chemicals, 99%) as a precursor and commercial γ -Al₂O₃ (SASOL Germany GmbH) as a support material.⁴⁹ After impregnation, the sample was calcined at 500 °C for 2 h in static air. The catalytic activity was evaluated by feeding a gas mixture of 3000 ppm CO, 1000 ppm NO, 1000 ppm C₃H₆, 5400 ppm O₂, 3% H₂O, and He in balance (stoichiometric three-way reaction condition, $\lambda \approx 1$) with a total flow of 50 ml/min at atmospheric pressure (GHSV = 60 000 h⁻¹). The light-off/light-out experiments (heating-/cooling-cycle) were performed between 40 °C and 800 °C with a temperature ramp of 10 °C/min.

The 0.5% Fe/SiO₂ catalyst was prepared by flame spray pyrolysis from a 1.0 mol/L solution of iron(III) acetylacetonate (Acros Organics, 99%) and tetraethyl orthosilicate (Alfa Aesar, 99.9%) in xylene (VWR chemicals).⁵⁰ For *operando* studies, either He, 90% CH₄/He, or 20% O₂/He at atmospheric pressure with a total gas flow of 5 ml/min was dosed (GHSV = 29 000 h⁻¹).

The chemical contents of catalyst samples were determined using a triple determination via inductively coupled plasma optical emission spectroscopy (ICP-OES) on an iCAP 7600 Duo spectrometer (Thermo Fischer Scientific).

B. Pd/Al₂O₃ three-way catalyst

As a first case study for demonstrating the use of the new setup in typical *operando* investigations in heterogeneous catalysis, *operando* XAS was conducted at the Pd K-edge (24 350 eV) for a Pd/Al₂O₃ catalyst during transient light-off/light-out measurements between room temperature and 800 °C under usual reaction conditions of a three-way catalyst (TWC). TWCs are widely applied for emission control of gasoline powered vehicles, to simultaneously convert CO, HC, and NO_x into CO₂, H₂O, and N₂. The active components in TWCs are precious metals, such as Pt, Pd, or Rh, and the support materials are mostly γ -Al₂O₃, CeO₂, and ceria-based composite oxides.³⁶ Despite the extensive application of TWCs, the reaction mechanism, the structural variation of the noble metal sites, and the noble metal-support are still debated in the literature.^{51,52} Hence, applying *operando* methods like XAS to elucidate the catalyst behavior under reaction conditions is highly relevant. In the present study, EXAFS spectra were recorded at room temperature in static air before exposure to the reaction mixture to characterize the initial state of the catalyst. Afterward, the cell was heated from room temperature to 800 °C with a temperature ramp of 10 °C/min and cooled down with the same temperature ramp. During the light-off/light-out cycle, XANES spectra were recorded under stoichiometric reaction conditions, which allowed us to monitor the change in the metal oxidation state. Pd K-edge XANES and EXAFS spectra as well as the Fourier transformed EXAFS spectra recorded at room temperature at different reaction conditions before and after catalytic tests are shown in Fig. 4. The XANES and EXAFS spectra of the as prepared sample in static air and in the reaction mixture at room temperature resemble those of the PdO reference. Accordingly, the corresponding Fourier transformed EXAFS spectra [Fig. 4(c)] show two main backscattering peaks at around 1.5 Å and 3.0 Å, associated with the first (Pd–O) and second (Pd–Pd) coordination shells, respectively,

of a PdO-like phase. After the light-off/light-out cycle, the collected XANES and EXAFS data mainly indicated the formation of metallic Pd particles. The corresponding Fourier transformed (FT) EXAFS data showed a main backscattering peak around 2.5 Å, which was assigned to the first Pd–Pd coordination shell of metallic Pd.

Figure 5 depicts the *operando* XANES spectra at the Pd K-edge as recorded during the light-off/light-out cycle. The results show no significant change in the XANES profile during light-off [Fig. 5(a)] up to around 160 °C, where CO conversion started (Fig. 6). Above this temperature, a relatively sharp decrease of the white line was observed, indicating the reduction of Pd particles. A further increase of the reaction temperature to 800 °C led to complete Pd reduction, in line with similar studies on Pd-based TWCs.^{53,54} After reaching 800 °C, the sample was cooled to room temperature and hardly any changes were observed in the XANES region of Pd K-edge [Fig. 5(b)].

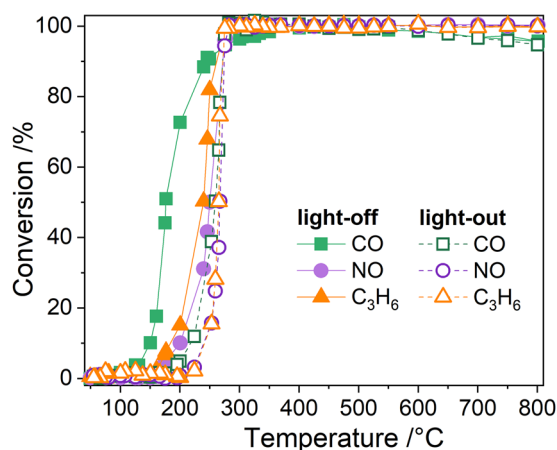


FIG. 6. Conversion of CO, NO, and C₃H₆ during light-off/light-out under stoichiometric three-way reaction conditions recorded via FTIR with the microreactor in parallel to the *operando* XAS measurements, $\lambda \approx 1$ (3000 ppm CO, 1000 ppm NO, 1000 ppm C₃H₆, 5400 ppm O₂, 3% H₂O, and He in balance), measured by online FTIR.

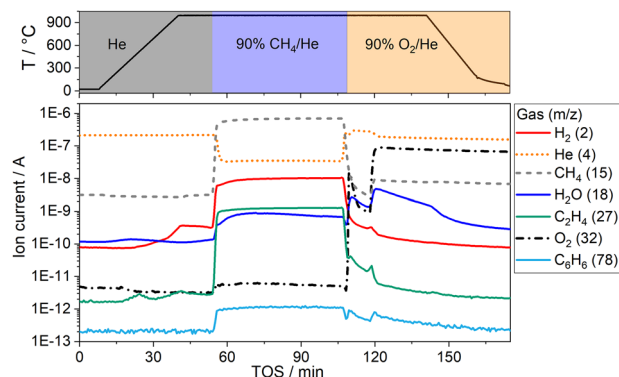


FIG. 7. Procedure of the *operando* experiment (top) and mass spectrometer signals (bottom) for 0.5% Fe/SiO₂ for heating up in He with 30 °C/min to 975 °C, 50 min reaction in 90% CH₄/He and oxidation in 20% O₂/He, and cooling down to 40 °C with 40 °C/min.

Simultaneously to monitoring of the catalyst structure, the TWC activity was measured by an online FTIR analyzer. The CO, C₃H₆, and NO conversion recorded during the light-off/light-out cycle of 2 wt. % Pd/Al₂O₃ is shown in Fig. 6. The results indicate an earlier oxidation onset for CO with a temperature of 50% conversion (T₅₀) at 170 °C. Around this temperature, Pd species were already partially reduced [Fig. 5(a)]. Only when CO is considerably oxidized (about 50% conversion) and Pd is almost completely reduced, C₃H₆ starts to convert and is immediately followed by NO reduction (T₅₀ at 240 °C and 250 °C, respectively). These activity trends are in line with previous studies on similar catalysts.

During the light-out activity test [Fig. 5(b)], an inverse hysteresis in CO conversion is observed with an increase of T₅₀ by about 90 °C. The T₅₀ variation could be due to the slight sintering and formation of metallic Pd particles during exposure to high temperatures. In contrast, a smaller inverse hysteresis is observed during the light-out of NO and C₃H₆ conversion, which shows a T₅₀ shifted by

20 °C toward the higher temperature. The smaller variation could be caused by the lower sensitivity of the NO reduction and C₃H₆ oxidation to the change in the Pd structure since distinct effects are known to appear for different reactions catalyzed by noble metal emission control catalysts.^{55,56}

C. Fe/SiO₂ for direct conversion of methane to olefins and aromatics

As a second case study, the 0.5% Fe/SiO₂ catalyst for direct non-oxidative conversion of methane was measured in fluorescence and transmission modes at the Fe K-edge (7112 eV). Recently discovered resources of methane increased the attention for processes which can directly convert methane into fuels and high value-added chemicals, such as ethylene and aromatics.⁵⁷ A newly proposed route, tackling remaining issues of low yield and stability, typically requires temperatures above 950 °C and low iron loading

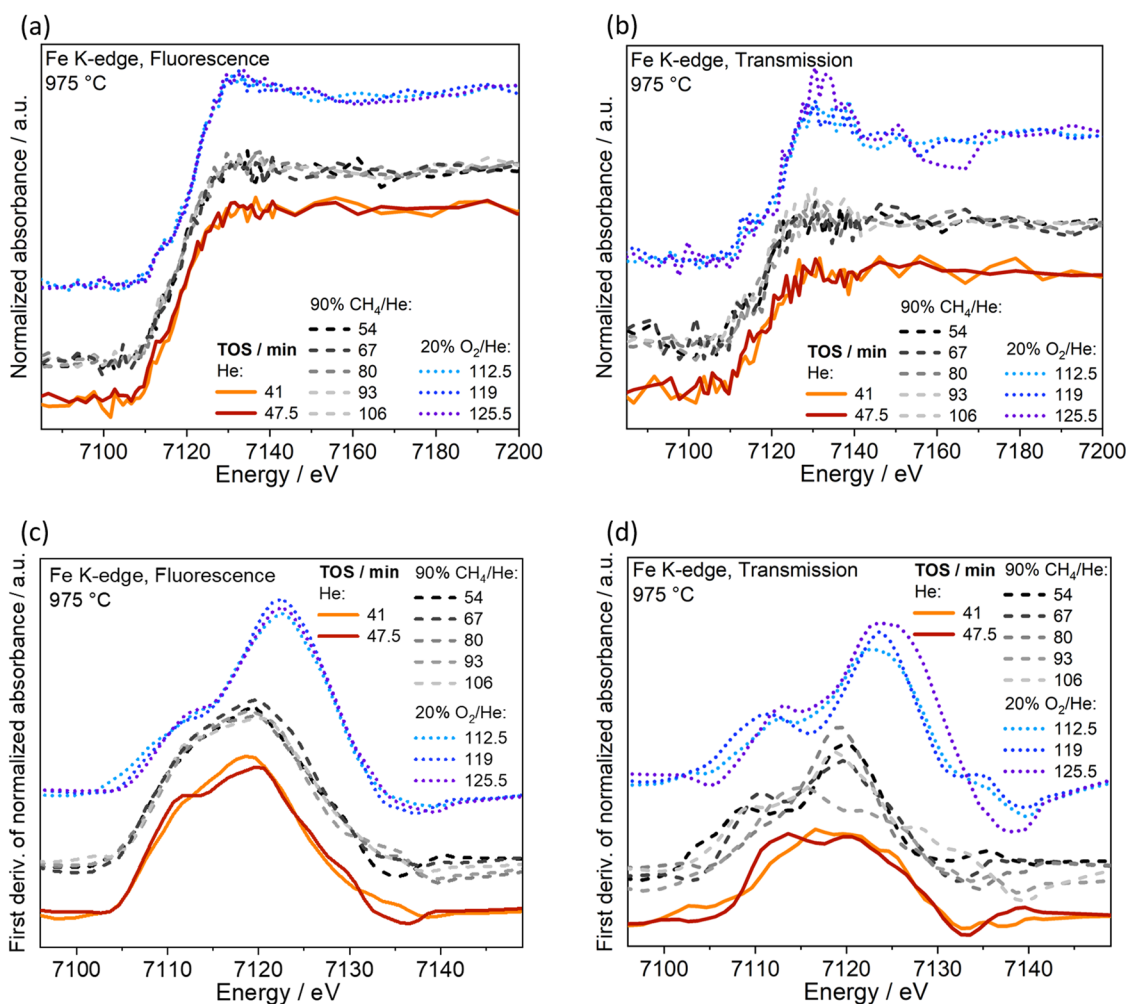


FIG. 8. (a) and (b) Normalized XANES spectra; (c) and (d) smoothed first derivative of XANES spectra at Fe K-edge of 0.5% Fe/SiO₂ at 975 °C reaction temperature in He (solid curve), 90% CH₄/He (dashed curve), and 20% O₂/He (dotted curve) atmosphere recorded in (a) and (c) fluorescence and (b) and (d) transmission modes.

(<1 wt. %) on SiO₂ supports.^{31–35} Hence, this application allows us to demonstrate the microreactor performance during *operando* XAS of catalysts with low loading of iron and high reaction temperatures (>900 °C). The applied *operando* measurement procedure with heating to 975 °C, reaction gas atmosphere in CH₄/He, switching to 90% O₂/He, and cooling to room temperature as well as the recorded MS signals are reported in Fig. 7. A linear heating ramp of 30 °C/min was conducted. As soon as the gas atmosphere is switched to methane, ethylene (*m/z* = 27) and aromatics (*m/z* = 78) are detected by the MS as reaction products. Additional MS signals of hydrocarbon product fragments are shown in Fig. S8.

During heating up in He, Fe undergoes a slight auto-reduction that has been already reported in the literature (cf. Fig. S9).⁵⁸ The XANES fluorescence measurements at different reaction conditions are shown in Fig. 8: at 975 °C, in the He atmosphere, Fe is in a highly reduced state, which barely changes during CH₄ conversion; the introduction of O₂ leads to a slight oxidation of Fe [Figs. 8(a) and 8(c)]. Simultaneous recording of transmission data during the reaction confirmed these findings, and they are not limited by the cell but rather by the low concentration of iron in the sample [Figs. 8(b) and 8(d)]. In fact, small differences as compared to the CH₄/He fluorescence data were observed in the derivative of the transmitted XANES spectra, which resulted from a lower signal-to-noise ratio of the transmission measurement due to the low Fe loading. Hence, for future experiments with similar sample parameters, the fluorescence mode seems to be more appropriate. Furthermore, additional in-depth studies are necessary to evaluate the nature of the active sites during methane conversion to higher alkenes and aromatics. This proof of concept demonstrates that the cell now opens up experiments at elevated temperatures for case studies, which are challenging even at lower temperatures, as for example, discussed for low-concentrated Fe-based catalysts during selective catalytic reduction of NO_x by ammonia in Ref. 59.

IV. CONCLUSION

A capillary plug-flow microreactor embedded in a wire heating system has been presented to conduct *operando* measurements at temperatures of up to 1050 °C. An efficient heating system results in a homogeneous temperature profile along the catalyst bed and sufficient pre-heating of the reactant gas. The advanced cell allows fast change of reaction temperatures with high heating/cooling rates (100 °C/min). Due to its relatively small size, the setup fits to the majority of synchrotron beamlines. The catalytic activity can be monitored by measuring the product gas composition with MS (used in the present study to evaluate the conversion of methane to ethylene and aromatics), FTIR (used to study the performance of the TWC catalyst), or gas chromatography. Avoiding iron in the setup and sufficiently shielding iron containing parts minimized interfering x-ray fluorescence signals from the surrounding iron and thereby allowed measurement of catalysts with iron loading below 0.5 wt. %. We verified this by comparing x-ray absorption spectra collected in transmission and fluorescence measurement modes for a 0.5% Fe/SiO₂ catalyst during direct conversion of methane under reaction conditions at 975 °C. Moreover, it was possible to measure Fe fluorescence of a 0.04% Fe/SiO₂ sample with 90% of the fluorescence signal originating from the sample. On the other hand, the reaction cell was successfully tested in *operando* XAS studies during

the operation of a 2% Pd/Al₂O₃ TWC at up to 800 °C for simultaneous removal of NO, CO, and C₃H₆, which will allow us to derive structure–activity correlations. The good quality of the XAS data obtained for such high x-ray absorbing elements combined with the broad temperature window covered by this microreactor cell is an essential parameter for understanding the functionality and also the deactivation behavior of TWC, which partly occurs at >1000 °C and is hardly accessible with present *operando* cell designs. Hence, the application of the cell might pave new possibilities for understanding the structure and mechanism of further catalysts during high temperature reactions like oxidative coupling of methane, dry and steam reforming, aromatization, and emission control. Moreover, the special design of the *operando* microreactor permits the study of processes conducted at elevated pressures and the combination of complementary characterization techniques, such as XRD and Raman spectroscopy, further extending its applicability.

SUPPLEMENTARY MATERIAL

See the [supplementary material](#) for energy-dispersive x-ray spectroscopy (EDX) and x-ray fluorescence (XRF) measurements of the Cu-ETP (CW004A) material and Kanthal A-1 heating wire, additional XANES spectra of 0.04% Fe/SiO₂-imp to evaluate the degree of background signals for x-ray fluorescence of the surrounding iron, and *operando* XANES measurements of the 0.5% Fe/SiO₂ sample during heating up in He to 975 °C reaction temperature.

ACKNOWLEDGMENTS

This work was supported by the German Research Foundation (Deutsche Forschungsgemeinschaft, DFG) through Grant No. GR 3987/9-1 [in kind cooperation with Xiulian Pan (Dalian Institute of Chemical Physics, China)] and through project CRC1441 (Project No. 426888090). Portions of this research were carried out at the light source PETRA III at DESY, a member of the Helmholtz Association (HGF). We would like to thank Edmund Welter and Ruidy Nemausat for assistance in using beamline P65. The authors thank Nilsu Öçeş (ITCP/KIT) for preparing technical drawings, Michael Zimmermann (IKFT/KIT) for EDX measurements, and the Institute for Beam Physics and Technology (IBPT/KIT) for the operation of the storage ring in the Karlsruhe Research Accelerator (KARA). Furthermore, the authors thank Kanthal GmbH, Germany, for providing resistive heating wires and Vasy Marchuk (ITCP/KIT) for beamtime support. Florian Perrin (ESRF) is acknowledged for his technical help at the early stages of the reactor design and Dr. Thomas Bergfeldt (IAM-AWP/KIT) for ICP-OES measurements.

DATA AVAILABILITY

The data that support the findings of this study are available within the article and its [supplementary material](#).

REFERENCES

- 1 G. Ertl, H. Knözinger, and J. Weitkamp, *Handbook of Heterogeneous Catalysis* (John Wiley & Sons, 1997).

- ²J. M. Thomas and W. J. Thomas, *Principles and Practice of Heterogeneous Catalysis* (John Wiley & Sons, 2014).
- ³D. Macquarrie, *Appl. Organomet. Chem.* **19**(5), 696 (2005).
- ⁴J.-D. Grunwaldt, J. B. Wagner, and R. E. Dunin-Borkowski, *ChemCatChem* **5**(1), 62–80 (2013).
- ⁵J. K. Nørskov, F. Studt, F. Abild-Pedersen, and T. Bligaard, *Fundamental Concepts in Heterogeneous Catalysis* (John Wiley & Sons, 2014).
- ⁶B. M. Weckhuysen, *Phys. Chem. Chem. Phys.* **5**(20), 4351–4360 (2003).
- ⁷K. F. Kalz, R. Kraehnert, M. Dvoyashkin, R. Dittmeyer, R. Gläser, U. Krewer, K. Reuter, and J.-D. Grunwaldt, *ChemCatChem* **9**(1), 17 (2017).
- ⁸B. R. Fingland, F. H. Ribeiro, and J. T. Miller, *Catal. Lett.* **131**(1), 1–6 (2009).
- ⁹J.-D. Grunwaldt and B. S. Clausen, *Top. Catal.* **18**(1-2), 37–43 (2002).
- ¹⁰S. R. Bare and T. Ressler, *Adv. Catal.* **52**, 339–465 (2009).
- ¹¹S. Bordiga, E. Groppo, G. Agostini, J. A. van Bokhoven, and C. Lamberti, *Chem. Rev.* **113**(3), 1736–1850 (2013).
- ¹²D. E. Doronkin, H. Lichtenberg, and J.-D. Grunwaldt, “Cell designs for *in situ* and *operando* studies,” in *XAFS Techniques for Catalysts, Nanomaterials, and Surfaces*, edited by Y. Iwasawa, K. Asakura, and M. Tada (Springer, 2017), pp. 75–89.
- ¹³A. M. Gänzler, M. Casapu, P. Vernoux, S. Loridant, F. J. Cadete Santos Aires, T. Epicier, B. Betz, R. Hoyer, and J.-D. Grunwaldt, *Angew. Chem., Int. Ed.* **56**(42), 13078–13082 (2017).
- ¹⁴D. Vantelon, P. Lagarde, A. M. Flank, E. Berrier, X. Secordel, S. Cristol, C. L. Fontaine, F. Villain, and V. Brioso, *Phase Transitions* **82**(4), 322–335 (2009).
- ¹⁵P. Sprenger, M. Stehle, A. Gaur, A. M. Gänzler, D. Gashnikova, W. Kleist, and J.-D. Grunwaldt, *ACS Catal.* **8**(7), 6462–6475 (2018).
- ¹⁶R. A. Dalla Betta, M. Boudart, K. Foger, D. G. Löffler, and J. Sánchez-Arrieta, *Rev. Sci. Instrum.* **55**(12), 1910–1913 (1984).
- ¹⁷F. W. H. Kampers, T. M. J. Maas, J. Van Grondelle, P. Brinkgreve, and D. C. Koningsberger, *Rev. Sci. Instrum.* **60**(8), 2635–2638 (1989).
- ¹⁸G. Meitzner, S. R. Bare, D. Parker, H. Woo, and D. A. Fischer, *Rev. Sci. Instrum.* **69**(7), 2618–2621 (1998).
- ¹⁹P. Riello, A. Lausi, J. Macleod, J. R. Plaisier, G. Zerauscek, and P. Fornasiero, *J. Synchrotron Radiat.* **20**(1), 194–196 (2013).
- ²⁰H. Huwe and M. Fröba, *J. Synchrotron Radiat.* **11**(4), 363–365 (2004).
- ²¹L. Nguyen, Y. Tang, Y. Li, X. Zhang, D. Wang, and F. Tao, *Rev. Sci. Instrum.* **89**(5), 054103 (2018).
- ²²G. Guilera, B. Gorges, S. Pascarelli, H. Vitoux, M. A. Newton, C. Prestipino, Y. Nagai, and N. Hara, *J. Synchrotron Radiat.* **16**(5), 628–634 (2009).
- ²³J.-D. Grunwaldt, M. Caravati, S. Hannemann, and A. Baiker, *Phys. Chem. Chem. Phys.* **6**(11), 3037–3047 (2004).
- ²⁴B. S. Clausen, G. Steffensen, B. Fabius, J. Villadsen, R. Feidenhans, and H. Topsøe, *J. Catal.* **132**(2), 524–535 (1991).
- ²⁵G. Sankar, J. M. Thomas, F. Rey, and G. N. Greaves, *J. Chem. Soc., Chem. Commun.* **1995**(24), 2549–2550.
- ²⁶J.-D. Grunwaldt, N. v. Vegten, A. Baiker, and W. v. Beek, *J. Phys.: Conf. Ser.* **190**, 012160 (2009).
- ²⁷A. Aguilar-Tapia, S. Ould-Chikh, E. Lahera, A. Prat, W. Delnet, O. Proux, I. Kieffer, J.-M. Basset, K. Takanabe, and J.-L. Hazemann, *Rev. Sci. Instrum.* **89**(3), 035109 (2018).
- ²⁸P. J. Chupas, K. W. Chapman, C. Kurtz, J. C. Hanson, P. L. Lee, and C. P. Grey, *J. Appl. Crystallogr.* **41**(4), 822–824 (2008).
- ²⁹S. J. A. Figueroa, D. Gibson, T. Mairs, S. Pasternak, M. A. Newton, M. Di Michiel, J. Andrieux, K. C. Christoforidis, A. Iglesias-Juez, and M. Fernández-García, *J. Appl. Crystallogr.* **46**(5), 1523–1527 (2013).
- ³⁰J. Andrieux, C. Chabert, A. Mauro, H. Vitoux, B. Gorges, T. Buslaps, and V. Honkimäki, *J. Appl. Crystallogr.* **47**(1), 245–255 (2014).
- ³¹X. Guo, G. Fang, G. Li, H. Ma, H. Fan, L. Yu, C. Ma, X. Wu, D. Deng, M. Wei, D. Tan, R. Si, S. Zhang, J. Li, L. Sun, Z. Tang, X. Pan, and X. Bao, *Science* **344**(6184), 616–619 (2014).
- ³²S. J. Han, S. W. Lee, H. W. Kim, S. K. Kim, and Y. T. Kim, *ACS Catal.* **9**, 7984–7997 (2019).
- ³³S. C. Oh, E. Schulman, J. Zhang, J. Fan, Y. Pan, J. Meng, and D. Liu, *Angew. Chem., Int. Ed.* **58**, 7083 (2019).
- ³⁴S. Sahoo, A. C. Reber, and S. N. Khanna, *Chem. Phys. Lett.* **660**, 48–54 (2016).
- ³⁵P. Šot, M. A. Newton, D. Baabe, M. D. Walter, A. P. van Bavel, A. D. Horton, C. Copéret, and J. A. van Bokhoven, *Chem. - Eur. J.* **26**, 8012 (2020).
- ³⁶R. M. Heck and R. J. Farrauto, *Appl. Catal., A* **221**(1-2), 443–457 (2001).
- ³⁷A. M. Gänzler, M. Casapu, F. Maurer, H. Störmer, D. Gerthsen, G. Ferré, P. Vernoux, B. Bornmann, R. Frahm, and V. Murzin, *ACS Catal.* **8**(6), 4800–4811 (2018).
- ³⁸J. J.-g. Hsia, *Experimental Investigation on the Reflectivity of Al, Cu, Zn and Ni and Its Comparison with Theory* (Purdue University, 1968).
- ³⁹L. Straka and S. Hašová, *Int. J. Adv. Manuf. Technol.* **97**(5-8), 2647–2654 (2018).
- ⁴⁰E. Welter, R. Chernikov, M. Herrmann, and R. Nemausat, *AIP Conf. Proc.* **2054**, 040002 (2019).
- ⁴¹A. Zimina, K. Dardenne, M. A. Denecke, D. E. Doronkin, E. Huttel, H. Lichtenberg, S. Mangold, T. Pruessmann, J. Rothe, T. Spangenberg, R. Steininger, T. Vitova, H. Geckeis, and J.-D. Grunwaldt, *Rev. Sci. Instrum.* **88**(11), 113113 (2017).
- ⁴²N. E. Tsakoumis, A. Voronov, M. Rønning, W. v. Beek, Ø. Borg, E. Rytter, and A. Holmen, *J. Catal.* **291**, 138–148 (2012).
- ⁴³M. Gentzen, D. E. Doronkin, T. L. Sheppard, A. Zimina, H. Li, J. Jelic, F. Studt, J. D. Grunwaldt, J. Sauer, and S. Behrens, *Angew. Chem., Int. Ed.* **58**(44), 15655–15659 (2019).
- ⁴⁴A. M. Gänzler, M. Casapu, A. Boubnov, O. Müller, S. Conrad, H. Lichtenberg, R. Frahm, and J.-D. Grunwaldt, *J. Catal.* **328**, 216–224 (2015).
- ⁴⁵S. Müller, A. Zimina, R. Steininger, S. Flessau, J. Osswald, and J.-D. Grunwaldt, *ACS Sens.* **5**(8), 2486–2496 (2020).
- ⁴⁶D. R. Lide, *CRC Handbook of Chemistry and Physics* (CRC Press, 2004).
- ⁴⁷D. Soulvong, S. Norsic, M. Taoufik, C. Coperet, J. Thivolle-Cazat, S. Chakka, and J.-M. Basset, *J. Am. Chem. Soc.* **130**(15), 5044–5045 (2008).
- ⁴⁸B. Ravel and M. Newville, *J. Synchrotron Radiat.* **12**(4), 537–541 (2005).
- ⁴⁹P. Lott, M. Eck, D. E. Doronkin, R. Popescu, M. Casapu, J.-D. Grunwaldt, and O. Deutschmann, *Top. Catal.* **62**(1-4), 164–171 (2019).
- ⁵⁰M. Høj, K. Linde, T. K. Hansen, M. Brorson, A. D. Jensen, and J.-D. Grunwaldt, *Appl. Catal., A* **397**(1-2), 201–208 (2011).
- ⁵¹J. Wang, H. Chen, Z. Hu, M. Yao, and Y. Li, *Catal. Rev.* **57**(1), 79–144 (2015).
- ⁵²D. Chatterjee, O. Deutschmann, and J. Warnatz, *Faraday Discuss.* **119**, 371–384 (2002).
- ⁵³Y. Lu, M. Santhosh Kumar, G. L. Chiarello, P. Dimopoulos Eggenschwiler, C. Bach, M. Weilenmann, A. Spiteri, A. Weidenkaff, and D. Ferri, *Catal. Commun.* **39**, 55–59 (2013).
- ⁵⁴M. Fernández-García, A. Iglesias-Juez, A. Martínez-Arias, A. Hungria, J. Anderson, J. Conesa, and J. Soria, *J. Catal.* **221**(2), 594–600 (2004).
- ⁵⁵E. Ogel, M. Casapu, D. E. Doronkin, R. Popescu, H. Störmer, C. Mechler, G. Marzun, S. Barcikowski, M. Türk, and J.-D. Grunwaldt, *J. Phys. Chem. C* **123**(9), 5433–5446 (2019).
- ⁵⁶A. Boubnov, S. Dahl, E. Johnson, A. P. Molina, S. B. Simonsen, F. M. Cano, S. Helveg, L. J. Lemus-Yegres, and J.-D. Grunwaldt, *Appl. Catal., B* **126**, 315–325 (2012).
- ⁵⁷P. Schwach, X. Pan, and X. Bao, *Chem. Rev.* **117**(13), 8497–8520 (2017).
- ⁵⁸D. Klukowski, P. Balle, B. Geiger, S. Wagloehner, S. Kureti, B. Kimmerle, A. Baiker, and J.-D. Grunwaldt, *Appl. Catal., B* **93**(1-2), 185–193 (2009).
- ⁵⁹M. Høj, M. J. Beier, J.-D. Grunwaldt, and S. Dahl, *Appl. Catal., B* **93**(1-2), 166–176 (2009).